Three-Dimensional Nanojunction Device Models for Photovoltaics

Artit Wangperawong[†] and Stacey F. Bent[‡,]*

Department of Electrical Engineering[†] and Department Chemical Engineering[‡],

Stanford University, Stanford, CA 94305

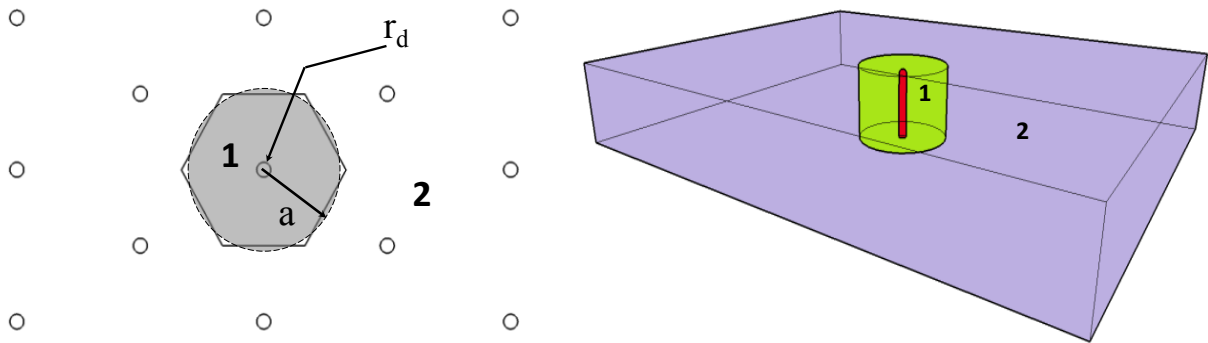**SUPPLEMENTARY INFORMATION**

Figure S1. The effective medium approximation accounts for diffusion to and collection at neighboring junctions outside of the unit cell **1**. As the hexagonal prism unit cell **1** approximates a cylinder, we can analytically solve the diffusion-collection equation in cylindrical coordinates by abstracting away the rest of the unit cells **2**. From the perspective of a unit cell **1**, the boundary conditions are determined by the average effect of the rest of the unit cells **2** of the device in which it is embedded. The unit cell has an electron diffusion length of L_1, and it interacts with a medium with an effective diffusion length L_2.

Solution for point-contact nanojunction: As shown in Fig. S1, we analyze regions **1** and **2** in cylindrical coordinates using an effective medium approximation (EMA) for region **2**. Assuming perfectly selective contacts on the top and bottom, Eq. (1) can be further reduced to an ordinary differential equation in a single dimension, r:

$$\frac{1}{r}\frac{\partial}{\partial r}\left(r\frac{\partial \varphi_m}{\partial r}\right) - \frac{1}{L_m^{\,2}}\varphi_m = 0 \qquad\qquad m = 1,2. \tag{2}$$

The boundary condition at the depletion edge, r_d, is taken to be

$$\varphi_1\left(r = r_d\right) = 1 \tag{3}$$

to represent collection surface, as electron-hole pairs generated in the depletion region are all assumed to be collected. The conditions at the cell boundary are

$$\varphi_1\left(r = a\right) = \varphi_2\left(r = a\right) \tag{4}$$

$$\left.\frac{\partial \varphi_1}{\partial r}\right|_{r=a} = \left.\frac{\partial \varphi_2}{\partial r}\right|_{r=a}. \tag{5}$$

The general solutions to Eq. (2) involve the zeroth order modified Bessel functions I_0 and K_0:

$$\varphi_1 = AI_0\left(\frac{r}{L_1}\right) + BK_0\left(\frac{r}{L_1}\right) \tag{6}$$

$$\varphi_2 = CI_0\left(\frac{r}{L_2}\right) + DK_0\left(\frac{r}{L_2}\right) \tag{7}$$

---

[*] Corresponding author: Stacey Bent, 381 North South Axis, Stanford University, Stanford, California 94305, USA, sbent@stanford.edu, Office: +1-650-723-0385, Fax: +1-650-723-9780

where A,B, C and D are constants and $D = 0$ in this application because φ_2 is finite as $r \to \infty$. The three remaining coefficients may be found by applying conditions (3)-(5), their solutions containing L_2 as an unknown variable.

Next we apply the definition of effective diffusion length[1], equating the photocurrent of the nanostructured cell under uniform photogeneration rate G_0 to that of a hypothetical homogenous and isotropic material with minority carrier diffusion length, L_e:

$$\int_V G_0 \varphi_{planar} dV = \sum_i^N \left\{ \int_{r_{j,i}}^{a_i} \int_0^h G_0 \varphi_1 dz \, 2\pi r \, dr \right\}$$
(8)

where $r_{j,i}$ is the position of the metallurgical junction of the ith unit cell of the N total unit cells comprising the device, h is the thickness of the cell, and

$$\varphi_{planar}(z) = \frac{\cosh((h - z)/L_e)}{\cosh(h/L_e)}$$
(9)

when the bottom contact is perfectly selective. Note that r_d reduces with applied forward bias, which is accounted for in the simulation results we present later. Eqns. 8 and 9 along with the boundary conditions contain the remaining unknown variable L_e. We can thus solve for L_2 by recognizing that for consistency all N unit cells are equivalent and that L_2 is equal to L_e. With L_2 known, φ for the entire device is determined. The ability to abstract away neighboring unit cells as a homogenous and isotropic medium is the essence of using an EMA.

In order to simulate the device performance, we assume a photogeneration rate $G(z)$ decaying exponentially with the penetration depth z at a rate given by the absorption coefficient of the material. We can obtain the photocurrent by integrating the product of the photogeneration and the collection probability over the volume of the unit cell as given by

$$I_{pc,i} = \int_{r_{j,i}}^{a_i} \int_0^h G(z)\varphi_1 dz \, 2\pi r dr$$

(10)

To obtain an I-V curve, we superimpose the photocurrent, the ideal dark current and the depletion region recombination current. By recognizing that φ is a solution to the diffusion equation, the reciprocal relationship between dark carrier distribution and photogenerated carrier collection allows us to calculate the ideal dark current $I_{dark,i}$ for each unit cell as

$$I_{dark,i} = -n_{p0} D_n \left[\int_0^h \frac{\partial \varphi_1}{\partial r}\bigg|_{r=r_d} 2\pi r_d dz \right] = -n_{p0} D_n \frac{\partial \varphi_1}{\partial r}\bigg|_{r=r_d} 2\pi r_d h$$

(11)

where n_{p0} and D_n are the equilibrium concentration and diffusivity of minority carriers in the absorber, respectively. The depletion region recombination current is

$$I_{dr,i} = -q \left[\int_{r_{j,i}}^{r_{d,i}} U_R(r) 2\pi r h dr \right], \quad U_R(r) = \frac{pn}{\tau(p+n)}$$

(12)

where $r_{d,i}$, p and n are functions of the applied bias and the potential from $r_{j,i}$ to $r_{d,i}$ is linearized. The lifetime τ in the depletion and quasi-neutral regions for both electrons and holes are the taken to be the same.

Following this approach, I-V curves are calculated using material properties of CdTe/CdS (Fig. 3). Assuming a type II heterojunction with no conduction band offset, additional consideration of barrier effects to current flow is not required.[2]

Solution for extended nanojunction: The solution for the extended nanojunction geometry is mathematically more sophisticated, as φ varies with both r and z. Nevertheless, the general procedure is identical to that of the point-contact geometry. We follow a procedure similar to that performed by Donolato for modeling multicrystalline solar cells[3]. Starting from Eq. (1), the

4

boundary conditions at the collection surface are

$$\varphi_1(r, z = 0) = 1,$$
(13)

$$\varphi_1(r = r_d, z) = 1$$
(14)

and at the cell boundary are

$$\varphi_1(r = a, z) = \varphi_2(r = a, z),$$
(15)

$$\left.\frac{\partial \varphi_1}{\partial r}\right|_{r=a} = \left.\frac{\partial \varphi_2}{\partial r}\right|_{r=a}$$
(16)

and at the back surface is

$$\left.\frac{\partial \varphi_m}{\partial r}\right|_{z=h} = 0,$$
(17)

where we again assume a perfectly selecting contact. Next we take the following integral

transformation of φ_m with respect to z:

$$\hat{\varphi}_m(r, k_n) = \int_0^h \varphi_m(r, z) \sin(k_n z) dz$$
(18)

where the eigenfunctions $\sin(k_n z)$ need to satisfy condition (17), so

$$k_n = \frac{\pi}{h}(2n+1) \qquad n = 0,1,2,3,... \tag{19}$$

To see this, consider the inverse transform

$$\varphi_m(r,z) = \frac{2}{h}\sum_{n=1}^{\infty}\hat{\varphi}_m(r,k_n)\sin(k_n z) \tag{20}$$

Applying condition (13) and the transformed functions, Eq. (1) reduces to the following ordinary differential equation:

$$\frac{1}{r}\frac{\partial}{\partial r}\left(r\frac{\partial \hat{\varphi}_m}{\partial r}\right) - \mu_{m,n}^{2}\hat{\varphi}_m + k_n = 0 \qquad m = 1,2 \tag{21}$$

where $\mu_{m,n} = \sqrt{1/L_m^{2} + k_n^{2}}$. The general solutions to (21) are

$$\hat{\varphi}_1 = \frac{k_n}{\mu_{1,n}^{2}} + A_n I_0\left(\mu_{1,n}r\right) + B_n K_0\left(\mu_{1,n}r\right) \tag{22}$$

$$\hat{\varphi}_2 = \frac{k_n}{\mu_{2,n}^{2}} + C_n I_0\left(\mu_{2,n}r\right) + D_n K_0\left(\mu_{2,n}r\right) \tag{23}$$

where A_n, B_n, C_n and D_n are coefficients of each term in the summation, and $D_n = 0$ because φ_2 is finite as $r \to \infty$. The remaining three coefficients may be found by applying conditions (14)-(16), their solutions containing L_2 as an unknown variable as was the case in the point-contact nanojunction. Also in a similar fashion to the point-contact nanojunction analysis, we use the EMA to solve for L_2, calculate the collection probability in the unit cell φ_1, calculate the dark

current based on the reciprocity theorem, integrate the product of photogeneration and φ_1 to get the photocurrent, calculate the depletion recombination current, and then model the I-V curve by superposition. Results are plotted in Fig. 3 along with the point-contact and planar geometries for comparison.

References

(1) C. Donolato, *Semicond. Sci. Technol.*, 13, 781, (1998).

(2) M. Gleockler, A. L. Fahrenbruch and J. R. Sites, Numerical modeling of CIGS and CdTe solar cells: setting the baseline, Proc. World Conf. Photov. Energy Conv., 3, 491 (2004).

(3) C. Donolato, *Semicond. Sci. Technol.* 15, 15 (2000).